Carbon supported Pt–NiO nanoparticles for ethanol electro-oxidation in acid media

Vanina Comignani [a], Juan Manuel Sieben [a, *], Maximiliano E. Brigante [b], Marta M.E. Duarte [a]

[a] Instituto de Ingeniería Electroquímica y Corrosión, CONICET, Universidad Nacional del Sur, B8000CPB Bahía Blanca, Argentina
[b] INQUISUR, Departamento de Química, Universidad Nacional del Sur, B8000CPB Bahía Blanca, Argentina

HIGHLIGHTS

- The electro-oxidation of EtOH on Pt–NiO/C catalysts was investigated in acid media.
- Small metal nanoparticles with sizes in the range of 3.5–4.5 nm were synthesized.
- Pt–NiO/C electrodes have better catalytic activity than Pt/C catalyst.
- The apparent activation energy for the overall reaction decreased with NiO content.
- Pt–NiO/C catalysts exhibited good long-term stability.

ARTICLE INFO

ABSTRACT

In the present work, the influence of nickel oxide as a co-catalyst of Pt nanoparticles for the electro-oxidation of ethanol in the temperature range of 23–60 °C was investigated. The carbon supported nickel oxide and platinum nanoparticles were prepared by hydrothermal synthesis and microwave-assisted polyol process respectively, and characterized by XRD, EDX, TEM and ICP analysis. The electrocatalytic activity of the as-prepared materials was studied by cyclic voltammetry and chronoamperometry. Small metal nanoparticles with sizes in the range of 3.5–4.5 nm were obtained. The nickel content in the as-prepared Pt–NiO/C catalysts was between 19 and 35 at.%. The electrochemical experiments showed that the electrocatalytic activity of the Pt–NiO/C materials increase with NiO content in the entire temperature range. The apparent activation energy ($E_{a,app}$) for the overall ethanol oxidation reaction was found to decrease with NiO content (24–32 kJ mol^{-1} at 0.3 V), while for Pt/C the activation energy exceeds 48 kJ mol^{-1}. The better performance of the Pt–NiO/C catalysts compared to Pt/C sample is ascribed to the activation of both the C–H and O–H bonds via oxygen-containing species adsorbed on NiO molecules and the modification of the surface electronic structure (changes in the density of states near the Fermi level).

© 2014 Elsevier B.V. All rights reserved.

1. Introduction

The limited amount of available resources, the high environmental impact and unequal access to resources conspire against the viability of the current energy model. To meet the growing energy demand of the world is necessary to develop and implement medium and long term energy strategies based on a more environmentally friendly and sustainable model. Clean and renewable energy can replace fossil fuels that pollute and fleece the natural resources, limiting the CO_2 and NO_x emissions and other chemical pollutants into the atmosphere, thereby reducing the greenhouse effect.

Within the clean technologies, fuel cells are widely recognized as a very attractive alternative to generate electricity cleanly and efficiently from a chemical reaction. In particular, the direct ethanol fuel cells (DEFCs) have a great potential as power sources for electric vehicles, secondary electricity generators and portable electronic devices such as notebooks, mobile phones, etc. [1]. Ethanol can be easily handled, stored and transported by using the existent fossil fuel infrastructure and it provides an energy density

very close to that of gasoline. Furthermore, ethanol is less toxic than methanol and has a less pronounced crossover through the ionomeric membrane due to their larger molecular size [2]. Furthermore, ethanol can be produced on a large scale from agricultural products and it is the major renewable biofuel obtained from the fermentation of biomass [3,4]. As well, the use of bioethanol can reduce the net carbon dioxide emissions nearly to zero.

However, there are some technical and economical barriers that have to be overcome to facilitate their massive production and commercialization in the global market, such as the high cost and scarcity of noble metals, the deficient activity and selectivity of anode electrocatalysts and the long term stability of the electrodes at temperatures compatible with available ionomeric membranes.

In recent years, several strategies have been undertaken for improving the catalytic properties of Pt-based systems and for increasing Pt utilization. To this purpose novel multi-metallic Pt nanoparticles have been developed, including alloy catalysts Pt–Rh–SnO$_2$/C [5], Pt-Ru-Mo [6], PtRuIrSn [7], PtSnM/C (M: Ni, Co, Rh and Pd) [8], and Pt-M oxides PtSnO$_x$ [9], PtCeO$_2$/C [10], Pt–MnO$_2$/C [11], Pt–RuO$_2$/C [12] and Pt–ZrO$_2$/C [13]. Furthermore, Pt-M (M: Cu, Ag and Co) bimetallic nanostructures with well-defined morphologies have attracted considerable attention because of their attractive structural features [14–16]. Another strategy to prepare highly active and durable catalysts with low Pt loading involves the production of nanoparticles with a core–shell structure [17–19].

In this article, we studied the influence of nickel oxide as a co-catalyst of Pt nanoparticles during the electrocatalytic oxidation of ethanol in acid media. Nickel, its hydroxides and oxides have been extensively used in several areas including fuel cells, energy storage, organic synthesis, waste water treatment, and electrochemical sensors because of their ability to catalyze reactions involving small organic molecules as well as their higher natural abundance and low-cost [[20], and references therein]. To the best of our knowledge, there are no articles dealing with the use of nickel oxide as a co-catalyst with platinum for the ethanol oxidation reaction in acid media. On the contrary, there are some works that evaluate the effect of NiO nanoparticles on Pt-based catalyst performance for methanol [21–23] and formic acid [24–26] electro-oxidation in acid media. Moreover, NiO has also been used as a co-catalyst to promote the electro-oxidation of methanol and ethanol in alkaline media on Pt and Pd particles [27–30].

Carbon supported nickel oxide and platinum nanoparticles were prepared and the synthesized Pt–NiO/C and Pt/C electrocatalysts were characterized by X-ray diffraction (XRD), energy dispersive X-ray spectroscopy (EDX), transmission electron microscope (TEM) and inductively coupled plasma atomic emission spectroscopy (ICP-AES). The electrocatalytic properties of the as-prepared samples were investigated by cycle voltammetry (CV) and chronoamperometry methods in the temperature range of 23–60 °C. The kinetic characteristics of the EOR process in function of changing temperature and applied potential were also investigated in detail.

2. Experimental section

2.1. Carbon support pretreatment

Pretreated Vulcan XC-72 R carbon black ($S_{BET} = 241$ m^2 g^{-1}, and $d_p = 40$ nm) was used as substrate. The carbon pretreatment was carried out in 5 M HNO$_3$ solution at 60 °C for 3 h. The slurry was then cooled and its pH value was adjusted to 7.0 with 0.5 M NaOH solution. The carbon powder was then filtered, washed with water and ethanol thoroughly and dried in an oven at 60 °C overnight.

2.2. NiO nanoparticles synthesis

Nickel(II) chloride hexahydrated, NaOH, KOH, KNO$_3$, HCl, and HNO$_3$ were obtained from Anedra. All chemicals were of analytical grade and used as received. Bidistilled water was used for the preparation of all solutions.

NiO nanoparticles were synthesized in alkaline medium by using a mixed-surfactant template composed by the cationic surfactant cetyltrimethylam-monium tosylate (CTAT, MW = 455.7 g mol^{-1}) and the amphiphilic copolymer Pluronic F68 (PEO$_{76}$PPO$_{29}$PEO$_{76}$, MW = 8400 g mol^{-1}, and PEO and PPO being the poly(oxyethylene) and the poly(oxypropylene) chain units, respectively). It is known that the use of surfactants as template provides homogeneity and monodispersity to the formed product with a significant decrease in the particle size. Briefly, 40 ml of Pluronic F68-CTAT (Polyoxyethylene-polyoxypropylene block copolymer and cetyl trimethylammonium tosylate) mixed solution was prepared with a 1:3 M ratio by adding the desired amount of the surfactant to water. This mixture was stirred in a conical flask at 35 °C to form a transparent template solution and then it was left at room temperature. At the same time, 11.6 ml of a 1.185 mol dm^{-3} NiCl$_2$ solution was prepared by adding the desired amount of the hydrated salt to water. To obtain the material 20 ml of NaOH 1.375 mol dm^{-3} was added drop by drop 15 min after the addition of the NiCl$_2$ solution to the surfactant solution. The final pH of the mixture was around 12. The resulting product, whose mole composition ratio was 1:2:0.0417:0.0014:289 NiCl$_2$:NaOH:CTAT:F68:H$_2$O, was stirred for 10 min and then left for 48 h in an autoclave at 100 °C. Then, the solid was filtered, washed with bidistilled water and left to dry at room temperature. Finally, it was calcined in an air flux by increasing the temperature from room temperature to 540 °C with a heating rate of 2 °C min^{-1}, and holding for 5 h at 540 °C.

2.3. Catalyst synthesis

The Pt–NiO/C catalysts with different nickel oxide contents (Table 1) were synthesized by microwave-assisted polyol process. The appropriate amount of nickel oxide and pretreated Vulcan XC-72R carbon black were dispersed into 50 ml of ethylene glycol (EG) in a beaker under ultrasonic treatment for 1 h to form uniform mixture inks. Then, H$_2$PtCl$_6$ aqueous solution (0.0386 mol dm^{-3}) was added into the uniform NiO/C dispersion. The suspension was ultrasonicated for 3 h and then the pH value adjusted to 10.0 by 1.0 ml of 1 mol dm^{-3} KOH-EG solution. The beaker was subjected to microwave heating (2450 MHz, 700 W) for 90 s. After cooling to room temperature, the pH value of the solution was adjusted to 7. The Pt–NiO/C catalysts were collected via suction filtration, washed repeatedly with bidistilled water and ethanol and finally dried overnight at 60 °C. A Pt/C catalyst was also synthesized by the same procedure for preparing Pt–NiO/C catalysts. The chemical reagents were of analytical grade and all electrodes were made to contain

Table 1
Nominal compositions of Pt–NiO/C and Pt/C catalysts and Pt loading in the activated carbon.

Catalysts	Nominal contents				Pt wt.%[c]
	Pt wt.%[a]	NiO wt.%[a]	Pt at.%[b]	Ni at.%[b]	
Pt/C	20	0	100	0	19.87
Pt–NiO/C1	20	2.5	79.0	21.0	20.00
Pt–NiO/C2	20	5.0	64.5	35.5	19.95

[a] Nominal contents of Pt and NiO in the activated carbon Vulcan.
[b] Nominal atomic ratios.
[c] Determined by ICP-AES analysis.

20 wt.% Pt loading on carbon.

2.4. Electrochemical characterization

Conventional three-compartment glass cells were used to run the electrochemical experiments with a PAR 273 potentiostat/galvanostat controlled by software ECHEM-M270 at temperature between 23 °C and 60 °C. The counter electrode was a platinum wire separated from the working electrode compartment by a porous glass diaphragm. The reference electrode was a saturated calomel electrode (SCE, +0.241 V vs. RHE) located in a Luggin capillary. The potentials mentioned in this work are referred to this electrode. Catalyst ink (1 mg ml^{-1}) was prepared as follows: 5 mg of catalyst powder were dispersed in 3.98 ml of bidistilled water, 1 ml of isopropyl alcohol and 20 μl of Nafion solution by sonication for 30 min. The working electrode was prepared by dispersing 20 μl of catalyst ink over the surface of a mirror polished glassy carbon rod (3 mm diameter). After that, the electrodes were dried at 60 °C for 30 min to ensure the catalyst binding to the glassy carbon support. All solutions were deaerated by bubbling N$_2$ for 30 min and then the inert atmosphere was maintained over the solution during the tests.

The characterization of the as-synthesized materials was carried out by cyclic voltammetry (CV) experiments in 0.5 mol dm^{-3} H$_2$SO$_4$ at a scan rate of 50 mV s^{-1}. The stable voltammograms were obtained after 30 cycles. Thereafter, the electrode activity for the alcohol electro-oxidation was evaluated in 1 mol dm^{-3} EtOH + 0.5 mol dm^{-3} H$_2$SO$_4$ solutions by applying a potential sweep at a scan rate of 50 mV s^{-1}. Stationary measurements (chronoamperometry) were performed applying pulses from an initial potential of 0 V for 15 min. Catalytic activity is displayed in terms of current per unit of active surface area and current per mass of Pt. The chemical stability of the most active sample was evaluated at a fixed potential (0.6 V) and 60 °C for 12 h.

The electroactive surface area (ESA) of the electrodes was measured by CO stripping technique with a Voltalab PGP201 potentiostat/galvanostat controlled by software VoltaMaster4. Briefly, an electrochemical glass cell filled with 0.5 mol dm^{-3} N$_2$-purged H$_2$SO$_4$ solution was saturated with CO for 20 min while the potential of the working electrode was maintained at −0.091 V. The excess of CO was then eliminated by bubbling with purified nitrogen, and finally the stripping voltammogram was recorded in the potential window of −0.091–0.8 V at a scan rate of 10 mV s^{-1} for 3 cycles. The stripping charges were determined between −0.091 V and 0.8 V after current background correction. The integration of the peak area corresponding to the CO stripping was used to determine the electroactive surface area, with the assumption of an adsorption ratio of a single CO molecule to each surface Pt atom and a monolayer charge of 420 μC cm^{-2}. In addition, the ESA was also determined from the electrical charge involved in hydrogen adsorption from voltammograms obtained in 0.5 M H$_2$SO$_4$, assuming that 1 cm^2 of smooth Pt requires 210 μC.

2.5. Physicochemical characterization

The morphology of the catalyst surface and the particle size were analyzed using transmission electronic microscopes (TEM) JEOL 100CX II and Tecnai F20 operated at 200 keV. The samples for TEM and HRTEM analysis were prepared by putting a drop of the catalyst ink on a standard copper grid. Bulk composition analysis was performed by an energy dispersive X-ray spectroscopy probe attached to a scanning electron microscope (SEM, JEOL 100). The samples were supported on GC disks and the analysis was done with the incident electron beam energies ranging from 0.1 to 20 keV.

X-ray diffraction (XRD) patterns of the as-prepared catalysts were recorded over the 2θ region of 30–80° using a Rigaku Dmax III C diffractometer with monochromated CuKα radiation source operated at 40 keV and 30 mA at a scan rate of 0.05° s^{-1}. Lattice parameters and crystallite size were determined by Rietveld analysis. The peak profiles in XRD patterns of the catalysts were fitted with the pseudo-Voigt function, using non-linear least-squares refinement procedures based on a finite difference Marquardt algorithm.

The amount of Pt deposited on the carbon substrate was estimated using inductively coupled plasma optical emission spectrometry ICP-AES (Shimadzu 1000 model III). For this purpose, 10.0 mg of each sample were digested in aqua regia for at least 8 h and filtered off to separate the carbonaceous material from the solution containing the metal ions. Furthermore, the amount of nickel dissolved into the ethanol solution was also measured by analyzing the electrolyte with ICP-AES spectroscopy, after potentiostatic long-term experiments.

3. Results and discussion

3.1. Structural characterization

Fig. 1 shows the XRD diffraction patterns of the as-prepared catalysts. Furthermore, the diffraction pattern of pure nickel oxide is shown in the inset of Fig. 1. The corresponding diffractograms of all catalysts presented three diffraction peaks centered at Bragg angles of about 40°, 47° and 68°, which can be assigned to the (111), (200) and (220) facets of the platinum face centered cubic (fcc) lattice structures. Particularly, the (111) reflection, the highest intensity peak for all catalysts, appeared at Bragg angles of 39.905°, 40.003 and 40.006° for Pt/C, Pt–NiO/C1 and Pt–NiO/C2, which correspond to d spacing in the range of 2.257–2.252 Å. The lattice constants of all as-prepared catalysts are included in Table 2. Importantly, the inspection of the XRD patterns strongly suggests that the presence of nickel oxide does not induce any structural change in the Pt network. Thus, the slight shift in the diffraction peaks could be attributed to the different size of the particles [31]. Furthermore, the ratio between (111), (200) and (220) areas does not change appreciably in these samples indicating the absence of any preferential orientation.

In addition, the other peaks observed at 2θ values of 37°, 43°, 63° and 75° in the diffractograms of PtNiO/C1 and Pt–NiO/C2 are assigned to the (111), (200), (220) and (311) planes of the NiO nanoparticles, respectively. Based on the information found in the JCPDS-database, the diffraction peaks can be indexed to a face centered cubic phase NiO (bunsenite phase) with a lattice parameter of 4.1776 Å. In addition, the (200) reflection peak is more intense than the others, suggesting a greater contribution from the {100} family of planes in the nanostructured material. This result is in agreement with previous studies [32,33].

The average Pt crystallite size (more properly, the coherence length of crystalline domains) was estimated from the (111) and (220) diffraction peaks by the Debye–Scherrer's equation [34]:

$$d_C = \frac{0.94\lambda_{K\alpha1}}{B_{2\theta}cos\theta_B} \tag{1}$$

where, $\lambda_{K\alpha1}$ is the wavelength of X-ray, θ_B is the angle of the peak, and $B_{(2\theta)}$ is the full width at half-maximum (FWHM) of the peak broadening in radians and the value 0.94 comes from considering spherical crystallite geometry (or cubo-octahedral shape). The average crystallite size of the Pt-based catalysts was found to be between 3.4 and 3.7 nm.

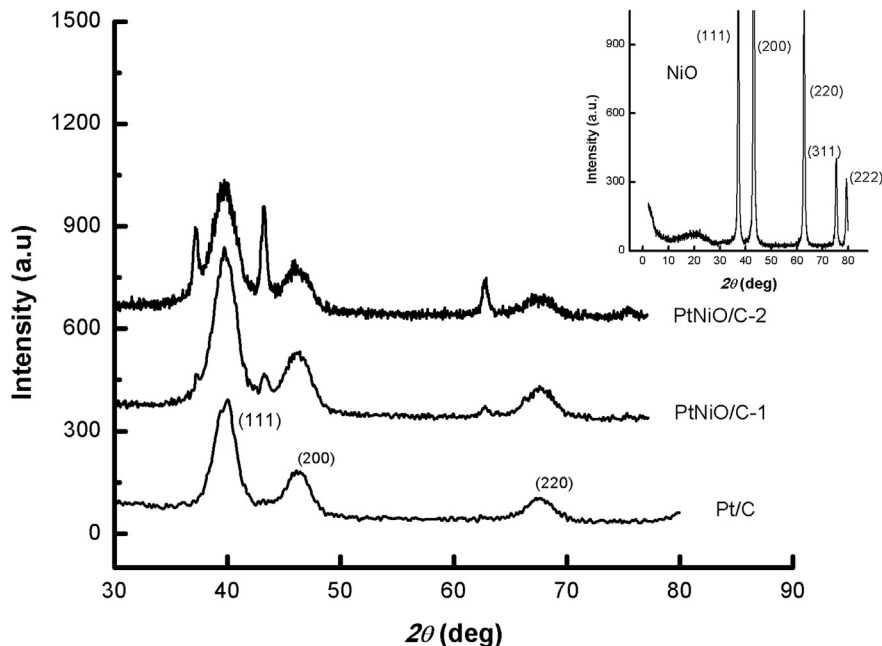The atomic composition of Pt–NiO/C catalysts was determined

Fig. 1. XRD patterns of Pt/C and Pt−NiO/C catalysts. Inset: XRD pattern of the pure NiO sample.

Table 2
Composition and characteristic parameters of Pt−NiO/C and Pt/C catalysts.

Catalysts	Pt at.%[a]	Ni at.%[a]	Pt:Ni ratio	a_{fcc} Å	d_c nm[b]	d_p nm[c]	ECSA m^2 g^{-1}[d]	η_{Pt} %
Pt/C	100	0	−	3.9139	3.7	4.5	59.8	78.9
Pt−NiO/C1	81.3	18.7	4.4	3.9122	3.6	4.3	62.5	80.2
Pt−NiO/C2	65.1	34.9	1.9	3.9124	3.4	4.1	64.9	78.8

[a] Atomic composition determined by EDX (±1.4 at%).
[b] Pt crystallite size from XRD using Debye−Scherrer equation (±0.3 nm).
[c] Mean particle size from TEM (±0.6 nm).
[d] Electrochemical surface area per unit mass determined from CO stripping technique and ICP-AES analysis (±2.1 m^2 g^{-1}).

by the EDX technique (see Fig. S1) and reported in Table 2. The Ni content in the as-synthesized catalysts in various parts of the powders is about 19 at.% and 35 at.% for Pt−NiO/C1 and Pt−NiO/C2 respectively, which is very close to the nominal value (Table 1). The distribution of C, Ni and Pt elements was also verified by EDX mapping from SEM images (Fig. S2). The Ni and Pt element mappings for a selected sample area revealed that the Pt−NiO/C catalysts have uniform element composition and dispersion, without any preferential element disposition.

Fig. 2 shows the representative TEM micrographies of the as-synthesized catalyst powders. More than one hundred particles were randomly measured in each sample to obtain the particle size distribution. The average particle sizes of all materials are reported in Table 2. The micrographies reveal the presence of a large amount of almost rounded nanoparticles with a relative narrow size distribution, which appear regularly distributed over the carbon support material. However, some small agglomerates with characteristic diameters in the range of 8−12 nm are also observed in all samples. Pt/C catalyst exhibits nanoparticles with an average diameter of 4.5 nm and a median of 4.2 nm. While, Pt−NiO/C1 and Pt−NiO/C2 have mean particle sizes of 4.3 and 4.1 nm with median values of 4.4 and 3.9 nm, respectively. The average particle sizes determined by TEM are in good agreement with the previous XRD

results. The latter suggests that the presence of NiO nanoparticles promotes the formation of smaller Pt nanoparticles during the microwave-assisted polyol process, which is in accordance with the results reported in the literature [35,36]. The reduction of the particle size is possible due to strong microwave absorption and faster heating of the carbon substrate after the addition of NiO nanoparticles, which is associated with a change in the dielectric constant and loss tangent of the carbon substrate [37]. A high resolution TEM (HRTEM) image of Pt−NiO/C catalyst reveals that Pt and NiO nanoparticles are in close contact (Fig. 2d).

3.2. Electrochemical characterization

Fig. 3a presents the steady cyclic voltammetry response of the Pt−NiO/C and Pt/C electrodes in 0.5 M H$_2$SO$_4$ solution. The curves for the as-prepared catalysts exhibited well defined hydrogen adsorption/desorption peaks in the potential range of −0.25 to 0.1 V. As can be noted, the electrodes Pt−NiO/C and Pt/C have essentially the same voltammetric features, *i.e.*, hydrogen adsorption/desorption and Pt oxide formation/reduction regions, although the voltammetric charge associated with these peaks is higher than that for Pt/C, reflecting the observed trend in the electrochemical surface area of the as-prepared catalysts. Moreover, the peak associated with the reduction of oxygenated surface species on Pt and the hydrogen adsorption peaks suffers a slight shift in the negative potential direction for Pt−NiO/C catalysts. This may be attributed to a modification in the strength of the Pt−O and Pt−H bonds in the presence of NiO or to differences in surface oxide reduction and hydrogen adsorption ability [38−40].

Fig. 3b shows the CO stripping voltammograms recorded at a sweep rate of 10 mV s^{-1} and room temperature. The electrochemical response of the as-prepared catalysts for CO$_{ads}$ stripping was evaluated by both the onset potential and the peak potential [41]. The onset of CO$_{ads}$ stripping starts at 0.38 V on Pt/C electrode, while CO$_{ads}$ oxidation begins at about 0.25 V on the NiO-containing Pt based catalyst. In addition, the stripping peak on the Pt−NiO/C electrodes locates at 0.45 V, which shift 80 mV to more negative potential compared with that on Pt/C (0.53 V). This means that the
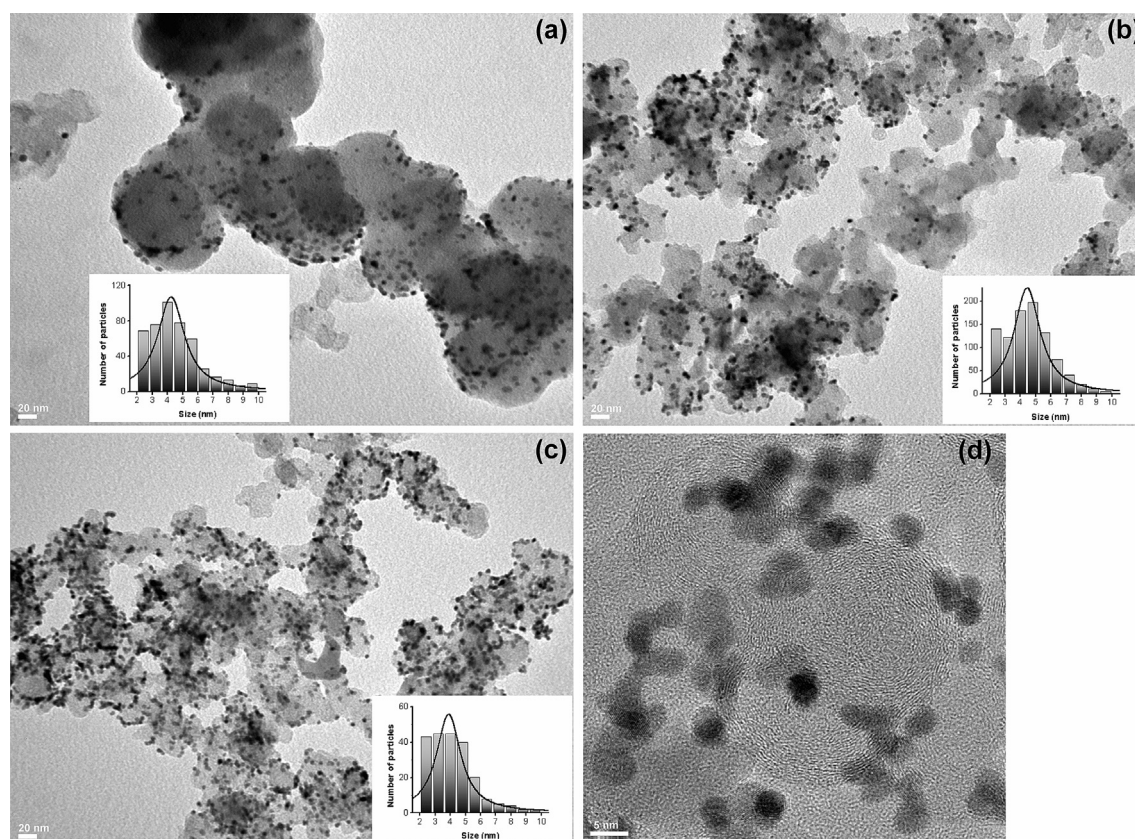
Fig. 2. TEM images and particle size distribution (inset) of the as-prepared electrocatalysts used in this work: (a) Pt/C, (b) Pt—NiO/C1 and (c) Pt—NiO/C2. (d) HRTEM image of Pt—NiO/C2 catalyst.
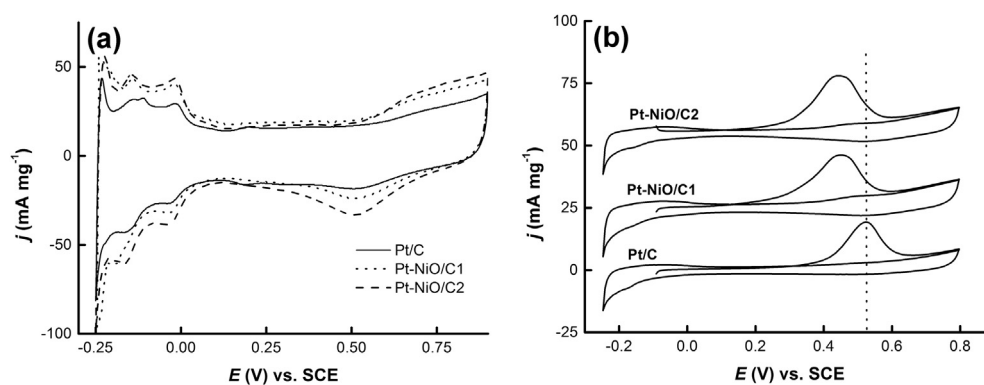

Fig. 3. (a) Steady cyclic voltammograms of the different carbon supported Cu@Pt—Ru core—shell catalysts in 0.5 M H_2SO_4 at room temperature and $\upsilon = 50$ mV s^{-1}. (b) Voltammetric curves for adsorbed CO stripping on the Pt/C, Pt—NiO/C1 and Pt—NiO/C2 electrocatalysts in 0.1 M H_2SO_4 at 10 mV s^{-1}.

removal of CO on the Pt—NiO/C electrodes is significantly easier than that on Pt/C catalyst, due to close proximity between Pt and NiO particles. It seems probable that the CO oxidation on Pt sites is facilitated via a bifunctional mechanism similar to that postulated for the Pt—Ru catalysts.

The electrochemical surface (ESA) of Pt/C, Pt—NiO/C1 and Pt—NiO/C2 was determined from both the electrical charge used in hydrogen adsorption and the stripping charge involved in CO_{ads} oxidation. The ESA values obtained by using the different procedures were very similar, indicating the accuracy of both techniques. The electrochemical surface area per unit mass (ECSA) of the as-prepared catalysts is reported in Table 2. The average ECSA

values calculated for Pt/C, Pt—NiO/C1 and Pt—NiO/C2 were 59.8 m^2 g^{-1}, 62.5 m^2 g^{-1} and 64.9 m^2 g^{-1} respectively.

Alternatively, the chemical surface area (CSA) of the platinum based catalysts in the absence of any screening or coalescence of crystals, i.e., assuming homogeneously distributed and spherical or cubic particles, can be calculated from the equation [42,43]:

$$CSA = \frac{6 \times 10^3}{\rho d_c} \tag{2}$$

where, ρ is the density of Pt (21.4 g cm^{-3}) and d_c (nm) is the mean crystallite size of the nanoparticles obtained from XRD. Therefore, the platinum utilization efficiency (η_{Pt}) can be estimated from

Equation (3):

$$\eta_{Pt} = \frac{ECSA}{CSA} \qquad (3)$$

The noble metal utilization efficiency for Pt-based catalysts is an important parameter because it reflects the number of available surface Pt sites for the electrochemical reactions. The calculation gives η_{Pt} values between 79 and 80%, indicating high degree of metal utilization (Table 2). This high Pt utilization is typical of the microwave-assisted ethylene glycol method of catalysts preparation [44,45].

3.3. Ethanol electro-oxidation

3.3.1. Potentiodynamic experiments

Fig. 4a shows the steady CV curves recorded for ethanol electro-oxidation at the as-prepared Pt–NiO/C and Pt/C electrodes at room temperature. Current densities for the alcohol electro-oxidation are normalized per milligram of Pt and per unit of active surface area (inset). As expected, in the presence of NiO the onset potential for the ethanol oxidation reaction (EOR) is shifted to lower potentials (between 0.1 and 0.15 V) with respect to Pt/C. The CV curves also point out that Pt–NiO/C2 electrode has the greatest activity for ethanol oxidation and the intensity of the anodic current during the
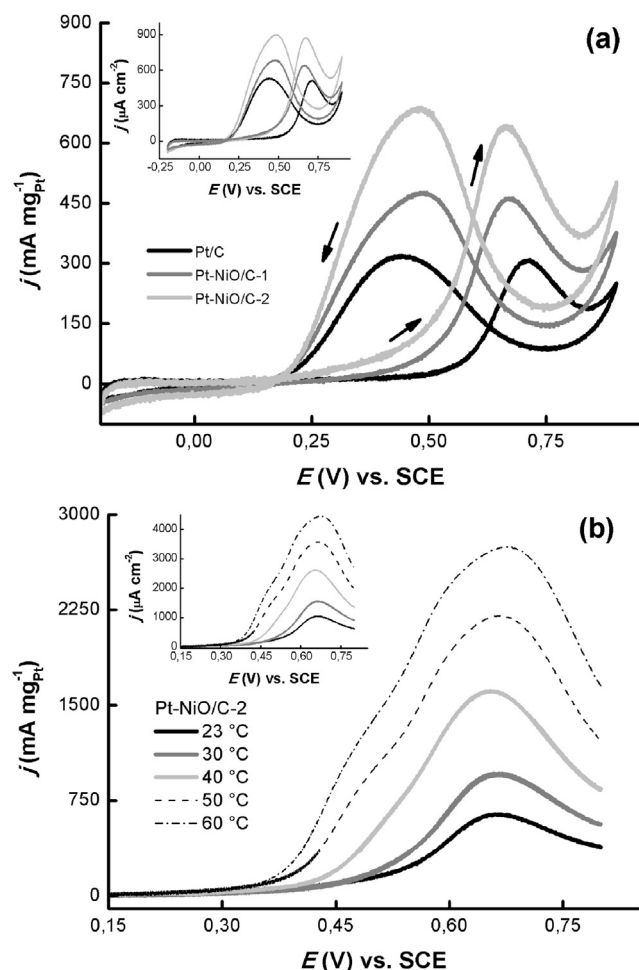

Fig. 4. (a) Steady cyclic voltammograms (thirtieth cycle) for the different electrodes in 1 M CH$_3$CH$_2$OH/0.5 M H$_2$SO$_4$ at room temperature. (b) Linear sweep voltammograms for ethanol oxidation on Pt–NiO/C2 electrode at various temperatures. The sweep rate was 50 mV s^{-1} and the arrows indicate the scan direction.

forward scan decrease in the order Pt–NiO/C2 > Pt–NiO/C1 > Pt/C. As can be seen, the presence of NiO leads to significant enhancements in the catalytic activity for the EOR in the region extended between 0.25 V and 0.55 V, a potential range relevant for fuel cells operation. The peak current density at Pt–NiO/C1 and Pt–NiO/C2 electrodes is reached at ca. 0.66 V, about 50 mV more negative than that at Pt/C, indicating that the alcohol oxidation is facilitated and needs less overpotential with these electrodes. Moreover, the peak current density of Pt–NiO/C1 and Pt–NiO/C2 is 1.5 and 2.1 times higher than that of Pt/C.

The effect of temperature in the catalytic activity of Pt–NiO/C2 electrode is shown in Fig. 4b. As can be noted, with increasing temperature, the onset potentials shift to slightly lower values. Moreover, the peak current density of Pt–NiO/C2 increases from 644 to 2750 mA mg^{-1} when the temperature rises from 23 to 60 °C due to the effect of temperature on the reaction kinetics of ethanol oxidation. The other catalysts depict similar trends for the electro-oxidation of ethanol but with lower activities. According to Sun et al. [46], the down-shift of the onset potential and the increase of current density with temperature is ascribed to higher reaction rate for complete oxidation of EtOH to CO$_2$ (i.e., the C–C bond scission becomes easier due to thermal activation) and smaller amounts of incomplete oxidation by-products (acetaldehyde and acetic acid). In addition, the facilitation of OH$_{ads}$ formation (water splitting) with increasing temperature can also contribute to the activity enhancement of ethanol oxidation [47,48].

3.3.2. Potentiostatic experiments

Cyclic voltammetry can only be used to obtain qualitative information concerning the electrocatalytic behavior of the supported catalysts during ethanol oxidation because these experimental conditions are transient in nature. More realistic reaction conditions can be obtained under potentiostatic conditions. Therefore, the electrocatalytic activity and the kinetic information of the electrodes in the oxidation of ethanol must be evaluated by using the information extracted from chronoamperometric experiments.

Current transient measurements at constant potentials were carried out for 900 s (Fig. S3). The mass-specific current densities obtained at three potentials (0.3 V, 0.4 V and 0.5 V) and at different temperatures on the as-prepared catalysts are given in Fig. 5. As expected, the resulting steady-state activities largely resemble those obtained in the voltammetric curves, but with lower current densities due to the partial blocking of the active sites by the accumulation of the poisoning species (CO, CH$_3$CHO, CH$_3$COOH, etc.) resulting from different reaction and diffusion rates [49,50]. The results indicate that the mass activities of EOR on Pt–NiO/C2 are, on average, between 1.9 and 3.3 times higher than that on Pt/C, which are in close agreement with CV results.

In order to assess the temperature dependence of ethanol electro-oxidation on the as-prepared catalysts, the apparent activation energies ($E_{a,app}$) were obtained at different potentials by linear regression of the Arrhenius plots (log j vs. $1/T$) showed in Fig. 6a–c. The $E_{a,app}$ values for ethanol oxidation on the electrodes are plotted versus the applied potential in Fig. 6d. For all catalysts the activation energy suffers a steady decrease as the potential increases, but this diminution is less pronounced from 0.4 V to 0.5 V. The apparent activation energies for the overall ethanol oxidation reaction are found to be in the order: Pt–NiO/C2 < Pt–NiO/C1 < Pt/C. For instance, at 0.3 V the apparent activation energy calculated from the Arrhenius plots vary with catalyst composition, showing a lower value around 24 kJ mol^{-1} for Pt–NiO/C2, and a higher value of 48 kJ mol^{-1} for platinum. In other words, the apparent activation energies of the EOR decrease with nickel oxide content. The energies obtained in the present work are
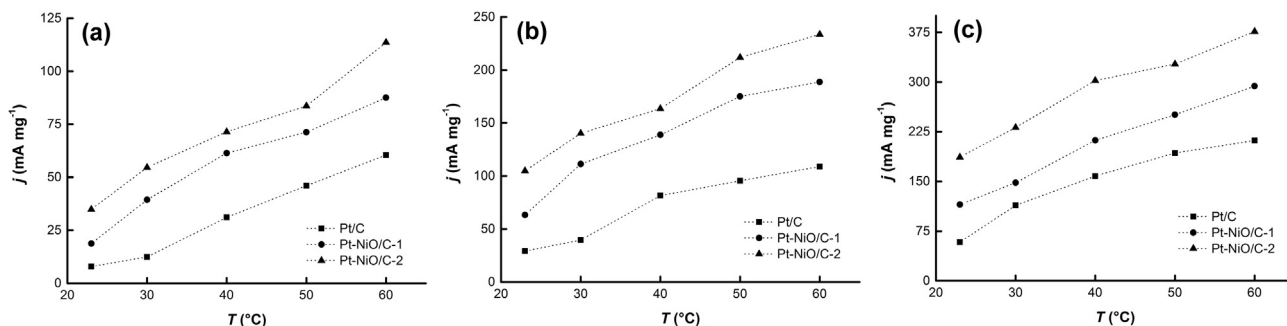
Fig. 5. Steady-state current densities during constant potential ethanol oxidation (1 M CH₃CH₂OH/0.5 M H₂SO₄) at different potentials and temperatures. (a) 0.3 V, (b) 0.4 V and (c) 0.5 V.
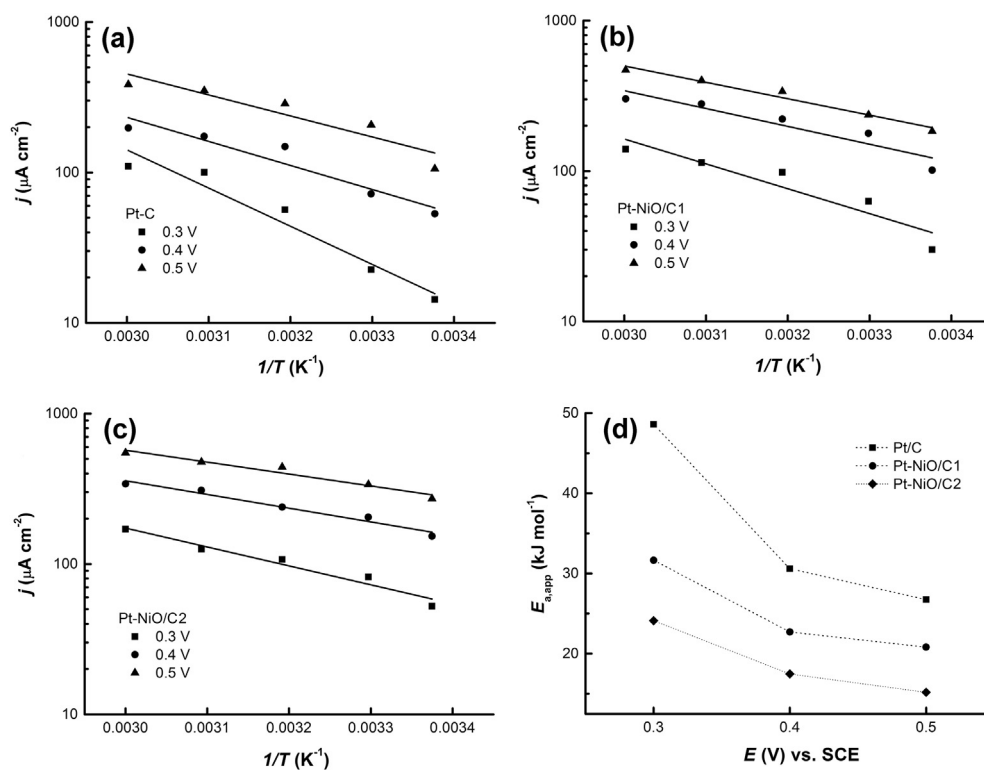
Fig. 6. Arrhenius plots of the overall ethanol oxidation rate in 1 M CH₃CH₂OH/0.5 M H₂SO₄ solution for Pt/C (a), Pt–NiO/C1 and Pt–NiO/C2 (c) at different potentials. (d) Apparent activation energies for the overall EOR at different potentials. Data taken from steady-state reaction currents.

comparable to those reported elsewhere for Pt [46,51] and Pt-based catalysts [6,52]. But, there are a little different from those energy values reported by other authors [53,54]. For instance, Colmati et al. [53] informed energy values of about 26, 31 and 42 kJ mol⁻¹ for the overall reaction on Pt/C, Pt–Ru/C and Pt₃–Sn/C electrodes at 0.4 V cell potential (c.a. 0.3 V vs. SCE in an anode) in the temperature range 70–100 °C. While, Gupta and Data [54] reported $E_{a,app}$ of around 37 kJ mol⁻¹ in potentiodynamic measurements for the overall reaction on several Pt–Sn/C catalysts at 0.3 V vs. SCE (temperature range 10–70 °C).

One should keep in mind, however, that the electro-oxidation of ethanol can proceed through different parallel paths (*i.e.*, formation of CO₂, CH₃CHO and CH₃COOH), which have different activation energies [46,55]. Therefore, in most cases, direct comparison is difficult because the experimental conditions reported in the literature are rather varied (*i.e.*, electrochemical setup, electrolyte concentration, temperature range, EtOH concentration, catalyst composition, etc.). Even so, the effect of NiO on the OER can be

evaluated through the information extracted from this kinetic analysis.

Despite the fact that a complete kinetic analysis was not performed, the rationalization of the Arrhenius plot analysis allow us to point out that the overall ethanol electro-oxidation process becomes more facilitated with the addition of nickel oxide into the catalyst. NiO nanoparticles may facilitate the oxidation of intermediates (e.g., adsorbed CO and CH₃CHO) at lower potentials than on Pt/C. This explanation agrees also with the results of the CO stripping voltammograms. Recent reports provided some evidence supporting this view. Park et al. [56,57] reported that the presence of NiO and Ni(OH)₂ on Pt/Ni and Pt/Ru/Ni electrodes enhances the ability of the catalyst to oxidize methanol molecules in acid media. The authors pointed out that these species could promote CO oxidation via a surface redox process. The role of nickel oxide in the electro-oxidation of formic acid on NiOₓ modified Pt and NiOₓ-Pt modified GC electrodes was evaluated by El-Nagar et al. [24,25]. The authors suggested that NiOₓ behaves as a catalyst mediator that

facilitate the charge transfer and/or remove the poisoning CO. Meanwhile, Liang et al. [58] and Wang et al. [59] indicated that the improved CO-tolerance of the PtRuNi/C electrodes can also be associated with a hydrogen spillover effect of nickel hydroxides on the catalyst surface (*i.e.*, the shift of H_{ads} on Pt sites to the neighboring nickel oxo-hydroxides). Whereas, Shen et al. [27,29] suggested that NiO can promote the oxidation of the poisoning intermediates as Ru does in Pt—Ru catalysts, that is OH_{ads} species formed on the surface of oxide promotes CO_{ads} oxidation.

Several studies reported in the literature claimed that the electro-oxidation of the alcohol at low temperatures and high EtOH concentration (≥ 1 mol dm^{-3}) leads to the formation of acetaldehyde and acetic acid with a small amount of CO_2, being CH_3CHO the main reaction product [9,60—62]. Thus, bearing our results in mind and comparing with those reported above, it seems probable that the nickel oxide particles promote the activation of both the C—H and O—H bonds of ethanol instead of the C—C bond scission. Hence, NiO would only act as an oxygen supplier at the interface between Pt and oxide nanoparticles. Besides, the proximity of NiO nanoparticles would modify the electronic structure of platinum at the Fermi level, weakening the reaction intermediate adsorption on the metal surface, thus reducing catalyst poisoning [49]. On the other hand, ethanol and acetaldehyde adsorbates could possibly react to form CO_{ads} or other $CH_{x,ads}$ intermediates via C—C bond breaking, and finally being oxidized to CO_2 at temperatures above 40 °C. However, more work should be done in order to confirm the role of NiO and evaluate the selectivity of the Pt—NiO/C catalysts. This will be the objective of our further investigation.

In order to evaluate the obtained results, a comparison with results reported in the literature should be carried out. In this regard, the employ of NiO as a co-catalyst on Pt-based systems used in the EOR reaction in acid media is not usually reported, being NiO combined with Pd or Pt one of the most studied systems in alkaline media [[63], and references therein]. The catalytic performance of the electrode with ~35 at% Ni (Pt—NiO/C2) in the temperature range 23—60 °C is really good when it is compared with other Pt-based materials containing different metals and metal oxides. For instance, Spinace et al. [64] and Parreira et al. [65] reported current densities in the range of 6—16 mA mg$_{Pt}^{-1}$ at 0.5 V vs. RHE for the EOR (1 M EtOH/0.5 M H_2SO_4) using different PtSnNi/C electrocatalysts at 25 °C. Recently, Beyhan et al. [8] stated a catalytic activity of 50 mA mg$_{Pt}^{-1}$ (0.15 mA cm$_{Pt}^{-2}$) at 0.5 V vs. RHE for PtSnNi/C electrodes in 1 M EtOH/0.1 M $HClO_4$ at room temperature. García et al. [6] studied ethanol electro-oxidation on PtRuMo catalysts with different Mo contents and reported catalytic activities between 0.02 and 0.15 mA cm$_{Pt}^{-2}$ at 0.5 V (RHE) in the temperature range 30—70 °C. Whereas, a catalytic activity of 197 mA mg$_{Pt}^{-1}$ at 0.6 V (NHE) for PtRu/TiO$_2$-embedded carbon nanofibers material in 2 M EtOH/0.5 M H_2SO_4 at room temperature has been reported elsewhere [61]. Silva et al. [66] prepared Pt$_3$Sn and PtSnO$_2$ catalysts of different alloying degree and reported catalytic activities of about 45 and 5 mA mg$_{Pt}^{-1}$ respectively for the EOR (1 M EtOH/0.5 M $HClO_4$) at 0.6 V (RHE) and room temperature.

Finally, the stability of the Pt—NiO/C catalysts was tested in potentiostatic experiments for 12 h at 0.6 V and 60 °C (not shown). Nickel ions were not detected by the ICP analysis of the 0.5 M H_2SO_4 + 1 M ethanol solution, indicating that nickel oxide nanoparticles in the Pt based catalysts are stable to corrosion in acidic media. A similar observation is reported elsewhere [56,57] in which nickel dissolution in acid media is inhibited in PtNi/C and PtRuNi/C catalysts after nickel hydroxide/oxide formation.

Considering the outstanding results obtained with the sample Pt—NiO/C2 and taking into account the good stability of the system, this material can be considered as a very promising catalyst for its use in the electro-oxidation of ethanol in acid media.

4. Conclusion

In this work, we have investigated the influence of NiO in the electro-oxidation of ethanol in acid media at carbon supported Pt catalysts in the temperature range 23—60 °C.

The CO stripping experiments indicate that the removal of CO on the Pt—NiO/C electrodes is significantly easier than that on Pt/C catalyst, which means that the close proximity between Pt and NiO particles facilitates the carbon monoxide oxidation via the bifunctional mechanism.

The CV curves and the potentiostatic experiments point out that catalytic activity for ethanol oxidation is increased in the order of Pt/C < Pt—NiO/C1 < Pt—NiO/C2, in the whole range of temperature. For all catalysts the activation energy suffers a steady decrease as the potential increases, but this diminution is less pronounced from 0.4 V to 0.5 V. The apparent activation energies for the overall ethanol oxidation reaction are found to be in the order: Pt—NiO/C2 < Pt—NiO/C1 < Pt/C. The better performance of the Pt—NiO/C catalysts compared to Pt/C sample is ascribed to the activation of both the C—H and O—H bonds via oxygen-containing species adsorbed on NiO molecules and the change in the density of states near the Fermi level on the Pt surface atoms. The better catalytic activity of Pt—NiO/C2 samples can be associated with an increasingly amount of C2 molecules instead of a more facilitated C—C bond breaking, which allows complete ethanol oxidation to CO_2.

Appendix A. Supplementary data

Supplementary data related to this article can be found at http://dx.doi.org/10.1016/j.jpowsour.2014.12.063.

References

[1] T. Iwasita, in: W. Vielstich, H.A. Gasteiger, A. Lamm (Eds.), Handbook of Fuel Cells Fundamentals, Technology and Applications, vol. 2, John Wiley & Sons, New York, 2003.

[2] S. Rousseau, C. Coutanceau, C. Lamy, J.M. Léger, Direct ethanol fuel cell (DEFC): electrical performances and reaction products distribution under operating conditions with different platinum-based anodes, J. Power Sources 158 (2006) 18—24.

[3] L.A. Rodríguez, M.E. Toro, F. Vazquez, M.L. Correa-Daneri, S.C. Gouiric, M.D. Vallejo, Bioethanol production from grape and sugar beet pomaces by solid-state fermentation, Int. J. Hydrog. Energy 35 (2010) 5914—5917.

[4] E.C. Petrou, C.P. Pappis, Bioethanol Production from Cotton Stalks or Corn Stover? A Comparative Study of Their Sustainability Performance, ACS Sustain. Chem. Eng. 2 (2014) 2036—2041.

[5] A. Kowal, M. Li, M. Shao, K. Sasaki, M.B. Vukmirovic, J. Zhang, N.S. Marinkovic, P. Liu, A.I. Frenkel, R.R. Adzic, Ternary Pt/Rh/SnO$_2$ electrocatalysts for oxidizing ethanol to CO$_2$, Nat. Mater. 8 (2009) 325—330.

[6] G. García, N. Tsiouvaras, E. Pastor, M.A. Peña, J.L.G. Fierro, M.V. Martínez-Huerta, Ethanol oxidation on PtRuMo/C catalysts: in situ FTIR spectroscopy and DEMS studies, Int. J. Hydrog. Energy 37 (2012) 7131—7140.

[7] K. Fatih, V. Neburchilov, V. Alzate, R. Neagu, H. Wang, Synthesis and characterization of quaternary PtRuIrSn/C electrocatalysts for direct ethanol fuel cells, J. Power Sources 195 (2010) 7168—7175.

[8] S. Beyhan, C. Coutanceau, J.-M. Léger, T.W. Napporn, F. Kadırgan, Promising anode candidates for direct ethanol fuel cell: carbon supported PtSn-based trimetallic catalysts prepared by Bönnemann method, Int. J. Hydrog. Energy 38 (2013) 6830—6841.

[9] L. Jiang, L. Colmenares, Z. Jusys, G.Q. Sun, R.J. Behm, Ethanol electrooxidation on novel carbon supported Pt/SnOx/C catalysts with varied Pt:Sn ratio, Electrochim. Acta 53 (2007) 377—389.

[10] L. Yu, J. Xi, CeO$_2$ nanoparticles improved Pt-based catalysts for direct alcohol fuel cells, Int. J. Hydrog. Energy 37 (2012) 15938—15947.

[11] S.K. Meher, G.R. Rao, Morphology-Controlled Promoting Activity of

Nanostructured MnO$_2$ for Methanol and Ethanol Electrooxidation on Pt/C, J. Phys. Chem. C. 117 (2013) 4888—4900.

[12] L. Cao, F. Scheiba, C. Roth, F. Schweiger, C. Cremers, U. Stimming, H. Fuess, L. Chen, W. Zhu, X. Qiu, Novel nanocomposite Pt/RuO$_2$ x H$_2$O/carbon nanotube catalysts for direct methanol fuel cells, Angew. Chem. Int. Ed. 45 (2006) 5315—5325.

[13] Y. Bai, J. Wu, J. Xi, J. Wang, W. Zhu, L.Q. Chen, X. Qiu, Electrochemical oxidation of ethanol on Pt-ZrO$_2$/C catalyst, Electrochem. Commun. 7 (2005) 1087—1094.

[14] M. Gong, G. Fu, Y. Chen, Y. Tang, T. Lu, Autocatalysis and Selective Oxidative Etching Induced Synthesis of Platinum—Copper Bimetallic Alloy Nanodendrites Electrocatalysts, ACS Appl. Mater. Interfaces 6 (2014) 7301—7308.

[15] G.T. Fu, R.G. Ma, X.Q. Gao, Y. Chen, Y.W. Tang, T.H. Lu, J.M. Lee, Hydrothermal synthesis of Pt—Ag alloy nanooctahedra and their enhanced electrocatalytic activity for the methanol oxidation reaction, Nanoscale 6 (2014) 12310—12314.

[16] J. Xu, X. Liu, Y. Chen, Y. Zhou, T. Lu, Y. Tang, Platinum—Cobalt alloy networks for methanol oxidation electrocatalysis, J. Mater. Chem. 22 (2012) 23659—23667.

[17] J.M. Sieben, A.E. Alvarez, V. Comignani, M.M.E. Duarte, Methanol and ethanol oxidation on carbon supported nanostructured Cu core Pt-Pd shell electrocatalysts synthesized via redox displacement, Int. J. Hydrog. Energy 39 (2014) 11547—11556.

[18] J.M. Sieben, V. Comignani, A.E. Alvarez, M.M.E. Duarte, Synthesis and characterization of Cu core Pt-Ru shell nanoparticles for the electro-oxidation of alcohols, Int. J. Hydrog. Energy 39 (2014) 8667—8674.

[19] A. Ammam, E.B. Easton, PtCu/C and Pt(Cu)/C catalysts: synthesis, characterization and catalytic activity towards ethanol electrooxidation, J. Power Sources 222 (2013) 79—87.

[20] Y. Miao, L. Ouyang, S. Zhou, L. Xu, Z. Yang, M. Xiao, R. Ouyang, Electrocatalysis and electroanalysis of nickel, its oxides, hydroxides and oxyhydroxides toward small molecules, Biosens. Bioelectron. 53 (2014) 428—439.

[21] R.S. Amin, R.M. Abdel Hameed, K.M. El-Khatiba, M. Elsayed Youssef, A.A. Elzatahry, Pt—NiO/C anode electrocatalysts for direct methanol fuel cells, Electrochim. Acta 59 (2012) 499—508.

[22] B. Park, E.J. Cairns, Electrochemical performance of TiO$_2$ and NiO as fuel cell electrode additives, Electrochem. Commun. 13 (2011) 75—77.

[23] D.B. Kim, H.J. Chun, Y.K. Lee, H.H. Kwon, H.I. Lee, Preparation of Pt/NiO-C electrocatalyst and heat-treatment effect on its electrocatalytic performance for methanol oxidation, Int. J. Hydrog. Energy 35 (2010) 313—320.

[24] G.A. El-Nagar, A.M. Mohammad, M.S. El-Deab, B.E. El-Anadouli, Facilitated Electro-Oxidation of Formic Acid at Nickel Oxide Nanoparticles Modified Electrodes, J. Electrochem. Soc. 159 (2012) F249—F254.

[25] G.A. El-Nagar, A.M. Mohammad, M.S. El-Deab, B.E. El-Anadouli, Electrocatalysis by design: enhanced electrooxidation of formic acid at platinum nanoparticles—nickel oxide nanoparticles binary catalysts, Electrochim. Acta 94 (2013) 62—71.

[26] M.K. Kumar, N.S. Jha, S. Mohan, S.K. Jha, Reduced graphene oxide-supported nickel oxide catalyst with improved CO tolerance for formic acid electrooxidation, Int. J. Hydrog. Energy 39 (2014) 12572—12577.

[27] P.K. Shen, C. Xu, Alcohol oxidation on nanocrystalline oxide Pd/C promoted electrocatalysts, Electrochem. Commun. 8 (2006) 184—188.

[28] F. Hu, C. Chen, Z. Wang, G. Wei, P.K. Shen, Mechanistic study of ethanol oxidation on Pd—NiO/C electrocatalyst, Electrochim. Acta 52 (2006) 1087—1091.

[29] C. Xu, P.K. Shen, Y. Liu, Ethanol electrooxidation on Pt/C and Pd/C catalysts promoted with oxide, J. Power Sources 164 (2007) 527—531.

[30] C. Xu, Z. Tian, P. Shen, S.P. Jiang, Oxide (CeO$_2$, NiO, Co$_3$O$_4$ and Mn$_3$O$_4$)-promoted Pd/C electrocatalysts for alcohol electrooxidation in alkaline media.

[31] C. Roth, M. Gotees, H. Fuess, Synthesis and characterization of carbon-supported Pt—Ru—WO$_x$ catalysts by spectroscopic and diffraction methods, J. Appl. Electrochem. 31 (2001) 793—798.

[32] M.A. Peck, M.A. Langell, Comparison of Nanoscaled and Bulk NiO Structural and Environmental Characteristics by XRD, XAFS, and XPS, Chem. Mater. 24 (2012) 4483—4490.

[33] I. Hotovy, J. Huran, L. Spiess, Characterization of sputtered NiO films using XRD and AFM, J. Mater. Sci. 39 (2004) 2609—2612.

[34] B.E. Warren, X-ray Diffraction, Addison-Wesley, Massachusetts, Reading, 1969.

[35] H. Chen, J. Duan, X. Zhang, Y. Zhang, C. Guo, L. Nie, X. Liu, One step synthesis of Pt/CeO$_2$—graphene catalyst by microwave-assisted ethylene glycol process for direct methanol fuel cell, Mater. Lett. 26 (2014) 9—12.

[36] P. Justin, G.R. Rao, Enhanced activity of methanol electro-oxidation on Pt—V$_2$O$_5$/C catalysts, Catal. Today 141 (2009) 138—143.

[37] E.A. Anumol, P. Kundu, P.A. Deshpande, G. Madras, N. Ravishankar, New insights into selective heterogeneous nucleation of metal nanoparticles on oxides by microwave-assisted reduction: rapid Synthesis of high-activity supported catalysts, ASC Nano 5 (2011) 8049—8061.

[38] J.K. Nørskov, J. Rossmeisi, A. Logadottir, L. Lindqvist, J.R. Kitchin, T. Bligaard, H. Jónsson, Origin of the overpotential for oxygen reduction at a fuel-cell cathode, J. Phys. Chem. B 108 (2004) 17886—17892.

[39] J.R. Kitchin, N.A. Khan, M.A. Barteau, J.G. Chen, B.Y.T.E. Madey, Elucidation of the active surface and origin of the weak metal—hydrogen bond on Ni/Pt(111) bimetallic surfaces: a surface science and density functional theory study, Surf. Sci. 544 (2003) 295—308.

[40] T. Toda, H. Igarashi, H. Uchida, M. Watanabe, Enhancement of the Electroreduction of Oxygen on Pt Alloys with Fe, Ni, and Co, J. Electrochem. Soc. 146 (1999) 3750—3756.

[41] F. Maillard, A. Bonnefont, M. Chatenet, L. Guétaz, B. Doisneau-Cottignies, H. Roussel, U. Stimming, Effect of the structure of Pt—Ru/C particles on CO$_{ad}$ monolayer vibrational properties and electrooxidation kinetics, Electrochim. Acta 53 (2007) 811—822.

[42] E.R. Savinova, F. Hahn, N. Alonso-Vante, The assessment of nanocrystalline surface defects on real versus model catalysts probed via vibrational spectroscopy of adsorbed CO, Surf. Sci. 603 (2009) 1892—1899.

[43] J.M. Sieben, M.M.E. Duarte, C.E. Mayer, Pt-Ru supported electrodes deposited by multiple successive cycles of potentiostatic pulses: evaluation of nafion film effect on methanol oxidation, J. Solid State Electrochem. 14 (2010) 1555—1563.

[44] S. Song, J. Liu, J. Shi, H. Liu, V. Maragou, Y. Wang, P. Tsiakaras, The effect of microwave operation parameters on the electrochemical performance of Pt/C catalysts, Appl. Catal. B 103 (2011) 287—293.

[45] F.J. Nores-Pondal, I.M.J. Vilella, H. Troianic, M. Granada, S.R. de Miguel, O.A. Scelza, H.R. Corti, Catalytic activity vs. Size correlation in platinum catalysts of PEM fuel cells prepared on carbon black by different methods, Int. J. Hydrog. Energy 34 (2009) 8193—8203.

[46] S. Sun, M.C. Halseid, M. Heinen, Z. Jusys, R.J. Behm, Ethanol electrooxidation on a carbon-supported Pt catalyst at elevated temperature and pressure: a high-temperature/high-pressure DEMS study, J. Power Sources 190 (2009) 2—13.

[47] J.L. Cohen, D.J. Volpe, H.D. Abruña, Electrochemical determination of activation energies for methanol oxidation on polycrystalline platinum in acidic and alkaline electrolytes, Phys. Chem. Phys. 9 (2007) 49—77.

[48] J.M. Sieben, M.M.E. Duarte, C.E. Mayer, Supported Pt and Pt—Ru catalysts prepared by potentiostatic electrodeposition for methanol electrooxidation, J. Appl. Electrochem 38 (2008) 483—490.

[49] J.M. Sieben, M.M.E. Duarte, Nanostructured Pt and Pt-Sn catalysts supported on oxidized carbon nanotubes for ethanol and ethylene glycol electrooxidation, Int. J. Hydrog. Energy 36 (2011) 3313—3321.

[50] A. Hamnett, in: A. Wieckowski (Ed.), Interfacial Electrochemistry, Marcel Dekker, New York, 1999, p. 843.

[51] E. Habibi, H. Razmi, Kinetics of direct ethanol fuel cell based on Pt-PoPD nano particle anode catalyst, Int. J. Hydrog. Energy 38 (2013) 5442—5448.

[52] S.S. Gupta, J. Datta, A comparative study on ethanol oxidation behavior at Pt and PtRh electrodeposits, J. Electroanal. Chem. 594 (2006) 65—72.

[53] F. Colmati, E. Antolini, E.R. Gonzalez, Effect of temperature on the mechanism of ethanol oxidation on carbon supported Pt, PtRu and Pt$_3$Sn electrocatalysts, J. Power Sources 157 (2006) 98—103.

[54] S.S. Gupta, S.S.J. Datta, Temperature effect on the electrode kinetics of ethanol electro-oxidation on Sn modified Pt catalyst through voltammetry and impedance spectroscopy, Mater. Chem. Phys. 120 (2010) 682—690.

[55] V. Rao, C. Cremers, U. Stimming, L. Cao, S. Sun, S. Yan, G. Sun, Q. Xin, Electro-oxidation of Ethanol at Gas Diffusion Electrodes A DEMS Study, J. Electrochem. Soc. 154 (2007) B1138—B1147.

[56] K.W. Park, J.H. Choi, B.K. Kwon, S.A. Lee, Y.E. Sung, H.Y. Ha, S.A. Hong, H. Kim, A. Wieckowski, Chemical and electronic effects of Ni in Pt/Ni and Pt/Ru/Ni alloy nanoparticles in methanol electrooxidation, J. Phys. Chem. B 106 (2002) 1869—1877.

[57] K.W. Park, J.H. Choi, Y.E. Sung, Structural, chemical, and electronic properties of Pt/Ni thin film electrodes for methanol electrooxidation, J. Phys. Chem. B 107 (2003) 5851—5856.

[58] Y. Liang, H. Zhang, Z. Tian, X. Zhu, X. Wang, B. Yi, Synthesis and structure-activity relationship exploration of carbon-supported PtRuNi nanocomposite as a CO-tolerant electrocatalyst for proton exchange membrane fuel cells, J. Phys. Chem. B 110 (2006) 7828—7834.

[59] Z.B. Wang, P.J. Zuo, G.J. Wang, C.Y. Du, G.P. Yin, Effect of Ni on PtRu/C catalyst performance for ethanol electrooxidation in acidic medium, J. Phys. Chem. C 112 (2008) 6582—6587.

[60] T.S. Almeida, K.B. Kokoh, A.R. De Andrade, Effect of Ni on Pt/C and PtSn/C prepared by the Pechini method, Int. J. Hydrog. Energy 36 (2011) 3803—3810.

[61] N. Nakagawa, Y. Ito, T. Tsujiguchi, H. Ishitobi, Improved reaction kinetics and selectivity by the TiO$_2$-embedded carbon nanofibers support for electro-oxidation of ethanol on PtRu nanoparticles, J. Power Sources 248 (2014) 330—336.

[62] S.Q. Song, W.J. Zhou, Z.H. Zhou, L.H. Jiang, G.Q. Sun, Q. Xin, V. Leontidis, S. Kontou, P. Tsiakaras, Direct ethanol PEM fuel cells: the case of platinum based anodes, Int. J. Hydrog. Energy 30 (2005) 995—1001.

[63] E. Antolini, Catalysts for direct ethanol fuel cells, J. Power Sources 170 (2007) 1—12.

[64] E.V. Spinace, M. Linardi, A. Oliveira Neto, Co-catalytic effect of nickel in the electro-oxidation of ethanol on binary Pt—Sn electrocatalysts, Electrochem. Commun. 7 (2005) 365—369.

[65] L. Silveira Parreira, J.C. Martins da Silva, M. D'Villa-Silva, F. Carmona Simões, S. Garcia, I. Gaubeur, M.A. Liutheviciene Cordeiro, E.R. Leite, M. Coelho dos Santos, PtSnNi/C nanoparticle electrocatalysts for the ethanol oxidation reaction: Ni stability study, Electrochim. Acta 96 (2013) 243—252.

[66] J.C.M. Silva, L.S. Parreira, R.F.B. De Souza, M.L. Calegaro, E.V. Spinacé, A.O. Neto, M.C. Santos, PtSn/C alloyed and non-alloyed materials: differences in the ethanol electro-oxidation reaction pathways, Appl. Catal. B 110 (2011) 141—147.